**ORIGINAL ARTICLE**

# Morphological, immunohistochemical, and genetic analyses of bronchiolar adenoma and its putative variants

Jinchen Shao[1], Jiani C Yin[2] , Hairong Bao[2], Ruiying Zhao[1] , Yuchen Han[1], Lei Zhu[1], Xue Wu[2], Yang Shao[2,3] and Jie Zhang[1]*

[1]*Department of Pathology, Shanghai Chest Hospital, Shanghai Jiao Tong University, Shanghai, PR China*
[2]*Nanjing Geneseeq Technology Inc., Nanjing, PR China*
[3]*School of Public Health, Nanjing Medical University, Nanjing, PR China*

*Correspondence to: Jie Zhang, Department of Pathology, Shanghai Chest Hospital, Shanghai Jiao Tong University, 241 West Huaihai Road, Shanghai 200030, PR China. E-mail: jiezhang49@outlook.com*

## Abstract

We collected 26 cases of bronchiolar adenoma (BA) and its variants, and performed a comprehensive characterization using a combination of morphological, immunohistochemical, and genetic assessments. Of these 26, 13 were classic bilayered cases, including 10 proximal and 3 distal-type BAs. Of note, we also identified 13 cases that lacked a continuous basal cell layer. In five cases, the adenomas were partially classic bilayered, leaving a single layer of columnar or cuboidal epithelial cells in some areas of the lesion (BA with monolayered cell lesions). In the other eight cases, the glandular or papillary structures were entirely composed of monolayered columnar or cuboidal epithelial cells, which were morphologically identical to the luminal epithelial cells of classic BA (monolayered BA-like lesions). Immunohistochemical analysis revealed thyroid transcription factor 1 expression by ciliated columnar epithelial cells, basal cells, and nonciliated columnar and cuboidal epithelial cells. Basal cells also expressed p40 and p63. Twenty-five cases underwent next-generation sequencing using a 422-cancer-gene panel (GeneseeqPrime). Oncogenic driver mutations were detected in 23 cases, including 13 (52%) with *EGFR* mutations, 4 (16%) with *KRAS* G12D/V mutations, 3 (12%) with *BRAF* V600E mutations, 2 (8%) with *ERBB2* exon 20 insertions, and 1 (4%) with a *RET* fusion. *EGFR* exon 20 insertions were present in 100% of BAs with monolayered cell lesions, 37.5% of monolayered BA-like lesions, and 8% of classic BA (Fisher's exact test, $p = 0.002$, false discovery rate = 0.014). Collectively, our study revealed a gradual morphological transition between BA and its variants. The genetic composition of BAs with monolayered structures differed significantly from those of classic BAs or lung adenocarcinoma.

Keywords: bronchiolar adenoma; monolayered lesions; next-generation sequencing; *EGFR* exon 20 insertions

## Introduction

A group of benign or putatively benign neoplasms derived from the bronchiolar epithelium, including ciliated muconodular papillary tumor (CMPT), peripheral glandular papilloma, and atypical bronchiolar hyperplasia, often challenge pathologists due to their confusing morphology and relatively low incidence, particularly during frozen section evaluation [1]. A recent study by Chang *et al* [2] redefined the concept of bronchiolar adenoma (BA) and categorized BAs into two main morphological subtypes, including proximal and distal, based on morphological similarities to the respective portions of the normal bronchiolar tree.

One major feature of BA lesions is a bilayered bronchiolar epithelium that consists of a luminal epithelial layer and a continuous basal cell layer. Such features form the basis for diagnosing BAs as benign tumors and differentiating them from lung adenocarcinomas. However, we found that a subset of BA cases exhibited monolayered columnar or cuboidal epithelial cells, with loss of the basal cell layer in some regions (hereafter referred to as BAs with monolayered cell lesions). We also found that some BA-like lesions

consisted entirely of monolayered bronchiolar epithelial cells with a complete loss of the basal cell layer (hereafter referred to as monolayered BA-like lesions). In this study, we collected 26 cases of BAs and its variants and performed morphological, immunohistochemical, and next-generation sequencing (NGS) analyses.

## Materials and methods

### Materials

Twenty-six patients with putatively benign bronchiolar epithelial lesions, who were admitted to our hospital and underwent surgical resection between 2015 and 2019, were retrospectively analyzed. Of those cases, 18 presented with BA, including 5 cases with partly monolayered cell lesions. The other eight cases showed entirely monolayered BA-like lesions. The study was conducted in accordance with the Declaration of Helsinki and was approved by the Ethical Review Board of Shanghai Chest Hospital. Informed written consent was obtained from each subject or their guardian.

### Methods

Surgical specimens were fixed in 10% neutral-buffered formalin, embedded in paraffin, serially cut into 4 mm-thick sections, and stained with hematoxylin–eosin. Each sample was histologically assessed by two experienced pathologists (JS and JZ).

#### Immunohistochemistry

Immunohistochemical analyses were performed on formalin-fixed paraffin-embedded (FFPE) sections from the surgically resected samples. The antibodies for immunohistochemistry (IHC) included anti-p63 (clone TP63/11, 1:300; Changdao Biotec., Shanghai, PR China), anti-thyroid transcription factor 1 (TTF1, clone SPT24, 1:200), anti-CK5/6 (clone D5/16B4, 1:300; QuanhuiImp & Exp Co., Shanghai, PR China), anti-p40 (rabbit polyclonal, 1:100), and anti-Ki-67 (clone UMAB 107, 1:300; Zhongshan Golden Bridge Bio., Beijing, PR China). IHC was performed on a Dako automated instrument (Dako Omnis; Agilent Technologies, Santa Clara, CA, USA) according to the manufacturer's instructions.

#### Molecular analysis

Samples from 25 patients underwent NGS using a panel of 422 cancer-related genes (GeneseeqPrime, see supplementary material, Table S1) in a Clinical Laboratory Improvement Amendments (CLIA)- and College of American Pathologists (CAP)-accredited laboratory (Nanjing Geneseeq Technology Inc., Jiangsu, PR China).

In brief, FFPE sections from resected samples and matched normal tissues were used for genomic DNA extraction using the QIAamp DNA FFPE Tissue Kit (QIAGEN, Hilden, Germany), according to the manufacturer's instructions. DNA quality was assessed using a NanoDrop 2000 spectrophotometer (Thermo Fisher Scientific, Waltham, MA, USA), and DNA quantity was measured using the dsDNA HS Assay Kit (Life Technologies, Carlsbad, CA, USA) on a Qubit 3.0 Fluorometer (Thermo Fisher Scientific, Waltham, MA, USA). Extracted tumor genomic DNA was fragmented into lengths of 350 bp using the Covaris M220 instrument (Woburn, MA, USA). Sequencing libraries were prepared using the KAPA HyperPrep kit (KAPA Biosystems, Wilmington, MA, USA) with optimized protocols. In brief, sheared DNA was subjected to end-repair, A-tailing, adaptor ligation, and size selection using Agencourt AMPcure XP beads (Beckman Coulter, Indianapolis, IN, USA).

Indexed DNA libraries were pooled, and hybridization capture was performed using custom biotinylated DNA probes (GeneseeqPrime; Nanjing Geneseeq Technology Inc.) targeting the coding regions of 422 cancer-related genes and the introns of fusion genes. Libraries were amplified using Illumina p5 and p7 primers (Illumina, San Diego, CA, USA) and KAPA HiFi HotStart Ready Mix, and were quantified using the KAPA library quantification kit (KAPA Biosystems, Roche Sequencing Solutions Inc., Pleasanton, CA, USA). The size distribution of the libraries was analyzed using the Agilent Bioanalyzer 2100 instrument with the High Sensitivity DNA kit (Agilent Technologies, Santa Clara, CA, USA). Capture-enriched libraries were sequenced on the Illumina HiSeq 4000 platform (San Diego, CA, USA). FASTQ files were aligned to the reference human genome (hg19) using the Burrows-Wheeler Aligner with modified parameters. Local realignment was performed using the Genome Analysis Toolkit (GATK, Broad Institute, Cambridge, MA, USA [3]). Single nucleotide polymorphisms (SNPs) and indels were observed by VarScan2 [4] and the Haplotype Caller/Unified Genotyper in GATK [3]. Common variants were removed using the dbSNP database and data from the 1000 Genomes project. Gene fusions were identified by FACTERA, and copy number variations were measured using ADTEx [5].

Table 1. Clinicopathological and mutational characteristics of 26 patients with lesions arising from the bronchiolar epithelium.

| ID | Age (years) | Sex | Lobe | Size (cm) | Subtype[†] | Surgical procedure | Frozen section diagnosis | Original diagnosis | Putative driver mutation | Other mutations | Follow-up (months) |
|---|---|---|---|---|---|---|---|---|---|---|---|
| 1 | 72 | M | Lower right | 0.5 | Proximal type (CMPT) | Lobectomy | Bronchiolar epithelial hyperplasia | Bronchiolar epithelial papillary hyperplasia with mucus retention | KRAS c.35G>T (p.G12V) | PPP2R1A c.779G>A (p.R260H) BMPR1A c.3_4delinsTA (p.MP1_?2) | 37 |
| 2 | 62 | F | Lower right | 0.6 | Proximal type (CMPT) | Wedge resection | Glandular epithelial hyperplasia with irregular structure | Bronchioloalveolar epithelial tumor-like hyperplasia; some mucin production | EGFR c.2311_2319dup (p.N771_H773dup) | MTOR c.6352C>T (p.L2118F) GATA3 c.1247T>C (p.M416T) | 25 |
| 3 | 60 | M | Lower right | 2 | Proximal type (CMPT) | Lobectomy | Invasive adenocarcinoma | CMPT | KRAS c.35G>A (p.G12D) | U2AF1 c.101C>T (p.S34F) TP53 c.524G>A (p.R175H) STAT3 c.547G>A (p.G183R) | 13 |
| 4 | 67 | M | Lower right | 0.7 | Proximal type (CMPT) | Wedge resection | Benign hyperplasia | CMPT | BRAF c.1799T>A (p.V600E) | PALLD c.G2421+1A | 11 |
| 5 | 74 | F | Lower right | 0.6 | Proximal type (CMPT) | Wedge resection | Invasive adenocarcinoma | CMPT | EGFR c.2237_2255delinsT (p.E746_S752>V) | RAC3 c.176C>T (p.A59V) | 16 |
| 6 | 64 | F | Lower right | 0.8 | Proximal type (CMPT) | Wedge resection | | CMPT | KRAS c.35G>A (p.G12D) | U2AF1 c.101C>T (p.S34F) | 11 |
| 7 | 53 | F | Middle right | 1.4 | Proximal type (CMPT) | Wedge resection | CMPT | CMPT | ERC1 intron4-RET:intron11 | – | 9 |
| 8 | 63 | F | Lower right | 1 | Proximal type (CMPT) | Wedge resection | CMPT | CMPT | Not detected | – | 11 |
| 9 | 68 | F | Lower right | 0.4 | Proximal type | Lobectomy | | Bronchiolar epithelial metaplasia | KRAS c.35G>T (p.G12V) | FGFR4 c.1261G>T (p.E421X) | 22 |
| 10 | 67 | F | Lower left | 0.7 | Proximal type | Wedge resection | AIS | AIS | BRAF c.1799T>A (p.V600E) | ERBB2 c.3568G>A (p.A1190T) | 31 |
| 11 | 74 | F | Lower right | 0.4 | Distal type | Wedge resection | Bronchioloalveolar epithelial hyperplasia | Bronchioloalveolar epithelial hyperplasia | Not detected | – | 21 |
| 12 | 61 | F | Lower right | 0.4 | Distal type | Segmentectomy | Bronchioloalveolar epithelial atypical hyperplasia | BA with B3-type thymoma | BRAF c.1799T>A (p.V600E) | PIK3R1 c.2018delA (p.N673TfsX19) | 11 |

*(Continues)*

Table 1. Continued

| ID | Age (years) | Sex | Lobe | Size (cm) | Subtype[†] | Surgical procedure | Frozen section diagnosis | Original diagnosis | Putative driver mutation | Other mutations | Follow-up (months) |
|---|---|---|---|---|---|---|---|---|---|---|---|
| 13 | 56 | M | Middle right | 0.3 | Distal type | Lobectomy | | Bronchiolar epithelial hyperplasia | EGFR c.2239_2264delinsGGAG (p.L747_A755>GD) | LHCGR c.1732G>A (p.D578N) ROS1 c.4379C>G (p.T1460S) | 34 |
| 14 | 53 | F | Lower right | 0.3 | Mixed type | Wedge resection | | Bronchiolar epithelial hyperplasia, some atypical hyperplasia | EGFR c.2311_2319dup (p.N771_H773dup) | – | 34 |
| 15 | 63 | F | Upper right | 0.4 | Mixed type | Lobectomy | | Bronchioloalveolar epithelial tumor-like hyperplasia | EGFR c.2313_2314insACA (p.N771_P772insT) | MCL1 Amp | 40 |
| 16 | 59 | F | Lower right | 0.3 | Mixed type | Wedge resection | Invasive adenocarcinoma | Invasive adenocarcinoma | EGFR c.2311_2319dup (p.N771_H773dup) | – | 28 |
| 17 | 47 | F | Upper right | 0.6 | Mixed type | Wedge resection | MIA | Bronchioloalveolar epithelial atypical adenocarcinoma-like hyperplasia | EGFR c.2311_2319dup (p.N771_H773dup) | – | 21 |
| 18 | 35 | F | Middle right | 0.7 | Mixed type | Lobectomy | Likely invasive adenocarcinoma | BA with malignant tumor | | | 9 |
| 19 | 60 | F | Lower right | 0.7 | Monolayered type | Lobectomy | | Invasive adenocarcinoma | EGFR c.2236_2250del (p.E746_A750del) | – | 12 |
| 20 | 59 | F | Lower right | 0.6 | Monolayered type | Lobectomy | AIS | AIS | ERBB2 c.2326delinsTTGT (p.G776delinsLC) | PTEN c.68del (p.L23*) JAK3 c.1192T>A (p.S398T) SETD2 c.7624G>T (p.E2542*) MED12 c.5746C>T (p.Q1916*) | 34 |
| 21 | 76 | F | Upper left | 0.9 | Monolayered type | Wedge resection | Likely adenocarcinoma | MIA | EGFR c.2155G>A (p.G719S) EGFR c.2303G>T (p.S768I) | MED12 c.5977C>T (p.Q1993*) | 11 |
| 22 | 28 | F | Middle right | 0.8 | Monolayered type | Wedge resection | Invasive adenocarcinoma | Invasive adenocarcinoma | EGFR c.2316_2317insTACAACCCC (p.P772_H773insYNP) | CTNNB1 c.860A>G (p.N287S) | 26 |

Table 1. Continued

| ID | Age (years) | Sex | Lobe | Size (cm) | Subtype[†] | Surgical procedure | Frozen section diagnosis | Original diagnosis | Putative driver mutation | Other mutations | Follow-up (months) |
|---|---|---|---|---|---|---|---|---|---|---|---|
| | | | | | | | | | | PIK3CA c.3141T>A (p.H1047Q) AKT1 c.49G>A (p.E17K) PALB2 c.3520G>A (p.G1174R) WT1 c.664C>T (p.R222C) | |
| 23 | 66 | F | Upper left | 0.5 | Monolayered type | Lobectomy | | CMPT | EGFR c.2300_2308dup (p.A767_V769dup) | – | 19 |
| 24 | 27 | M | Bottom left | 0.7 | Monolayered type | Wedge resection | AIS | AIS | EGFR c.2235_2240inv (p.E746_L747>IP) | PAX5 c.364C>T (p.R122W) | 18 |
| 25 | 49 | F | Lower left | 0.7 | Monolayered type | Lobectomy | MIA | MIA | EGFR c.2303_2311dup (p.S768_D770dup) | TP53 c.472C>T (p.R158C) | 17 |
| 26 | 72 | M | Middle right | 0.5 | Monolayered type | Wedge resection | MIA | MIA | ERBB2 c.2313_2324dup (p.Y772_A775dup) | NBN c.151A>G (p.N51D) KLLN c.413delA (p.H138fs) MCL1 Amp | 16 |

[†]Mixed type, double–layered BA with monolayered cells in some area of the lesion; monolayered type, BA-like lesions with entirely monolayered epithelial cells; AIS, adenocarcinoma in situ; MIA, minimally invasive adenocarcinoma.
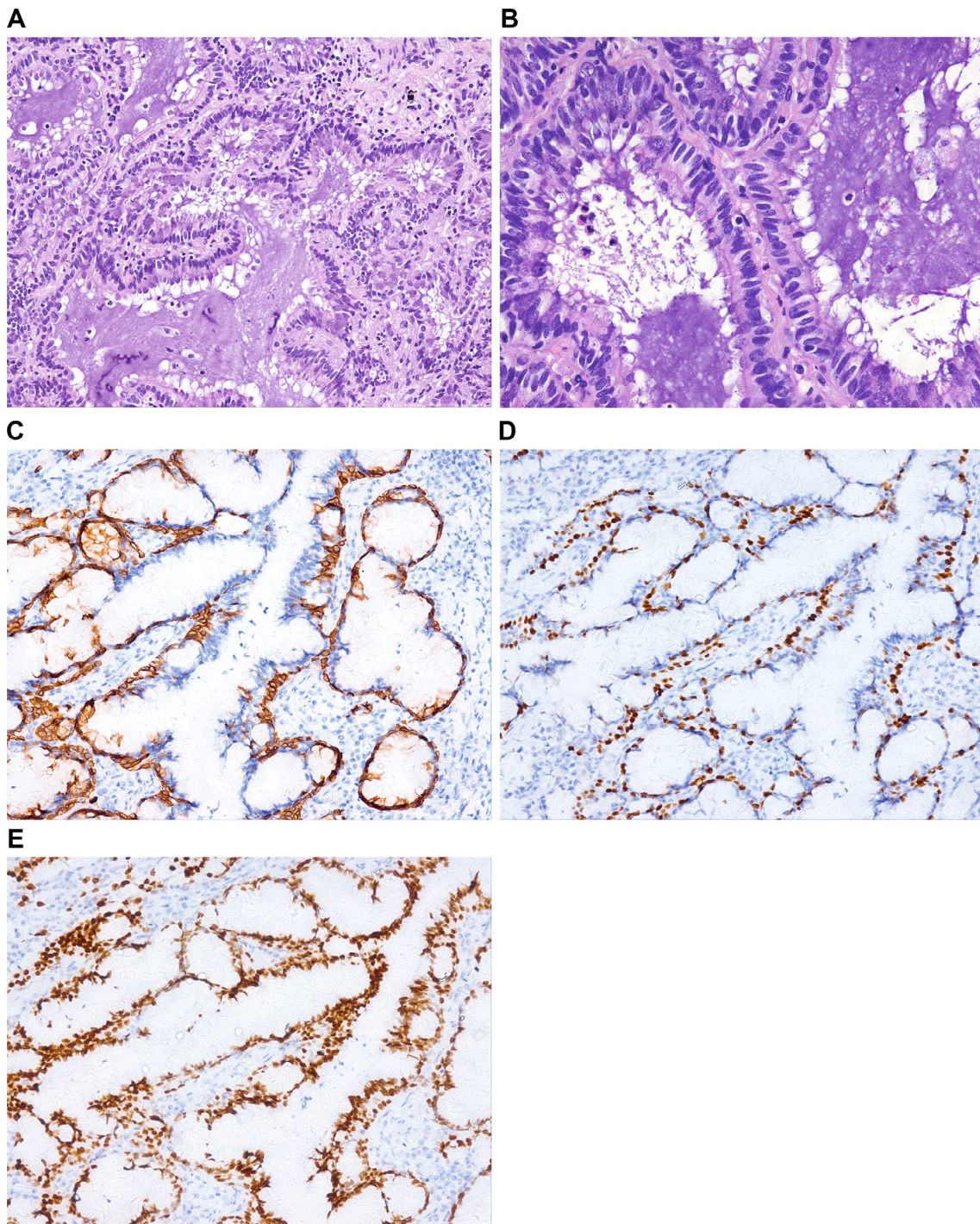
**Figure 1.** Morphological features of CMPT. (A) The bronchial lumen of CMPT is defined by papillary and glandular structures with abundant mucin. (B) Luminal cells are primarily ciliated columnar and mucinous cells. Clear ciliated structures can be seen on the apical surface of columnar cells. (C) CK5/6 expression is detected in basal cells. (D) p40 expression is detected in basal cells. (E) TTF1 expression is detected in the nonmucinous luminal cells and basal cells.
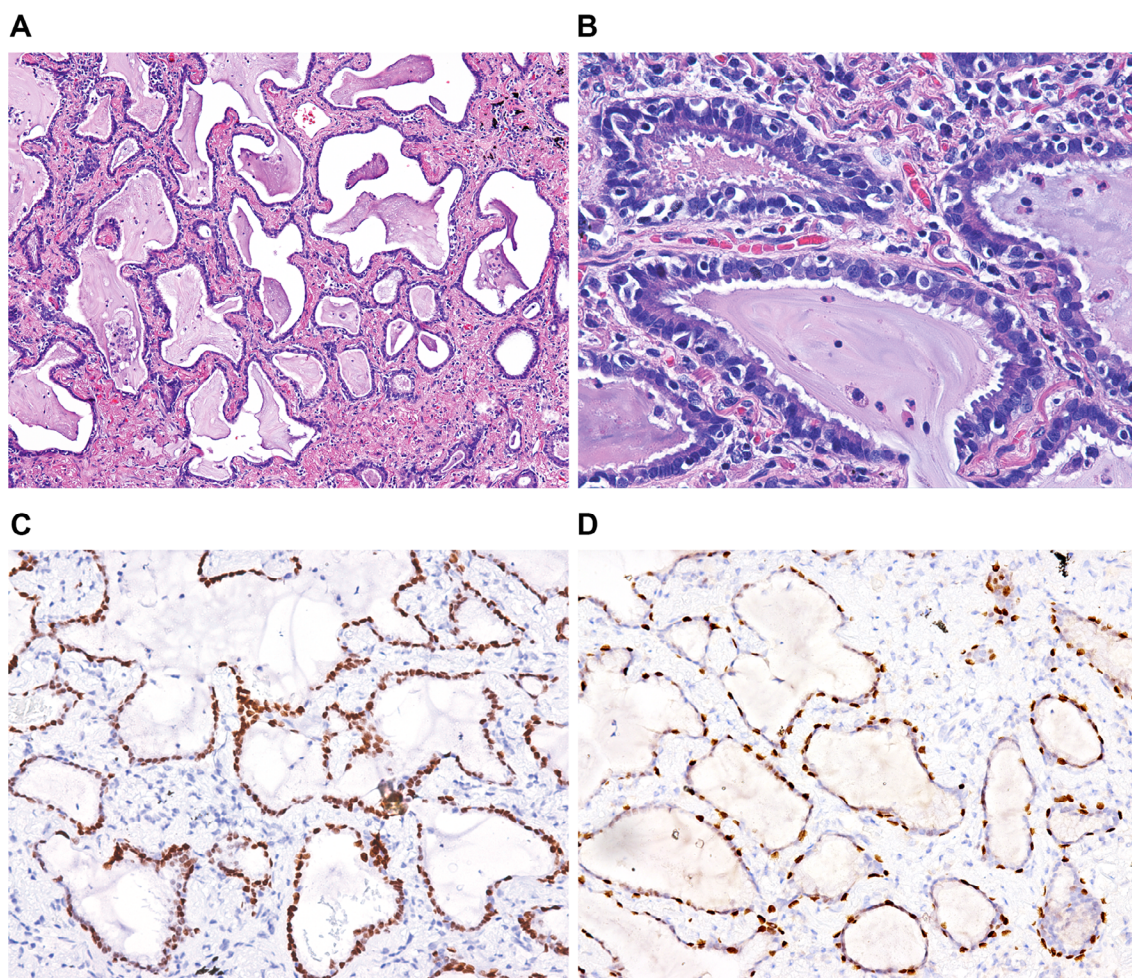
Figure 2. Morphological features of proximal–type BAs with flat architecture. (A) The architecture of such tumors is predominantly flat, and no papillary structures are observed. The glandular lumen is filled with mucin. (B) Luminal cells are primarily ciliated and mucinous. (C) TTF1 expression is detected in the nonmucinous luminal and basal cells. (D) p40 expression is detected in basal cells.

## Results

### Patient characteristics and radiological features

Detailed clinicopathological information for the entire cohort is provided in Table 1. Of the 26 patients analyzed, 6 were males and 20 were females, with a median age of 61 years at diagnosis. Sixteen patients underwent wedge resection or segmentectomy of the lung, while 10 underwent lobectomy. The mean follow-up time was 21 months and ranged from 9 to 40 months. None of the patients experienced disease recurrence or distant metastasis following surgical interventions.

Computed tomography (CT) imaging showed that 20 cases manifested as nodular ground-glass opacities of various sizes, 5 cases were solid nodules, and 1 case

was a lesion that was present with other pulmonary tumors and resected at the time of surgery but was undetectable by CT imaging. The nodules were of variable sizes, with diameters ranging from 0.3 to 2.0 cm. Twenty-one cases had clearly defined borders, while 5 cases were ill-defined with no clear border from the surrounding parenchyma.

### Histological and IHC findings

Among the 18 cases of BA, 11 were classified as proximal type, with 8 cases of CMPT and 3 cases of flat-type BA. CMPTs were characterized by papillary and glandular architecture, with abundant extracellular mucin production. CMPTs were composed of three types of epithelial cells, including ciliated columnar cells, mucinous cells, and basal cells. Ciliated columnar cells were
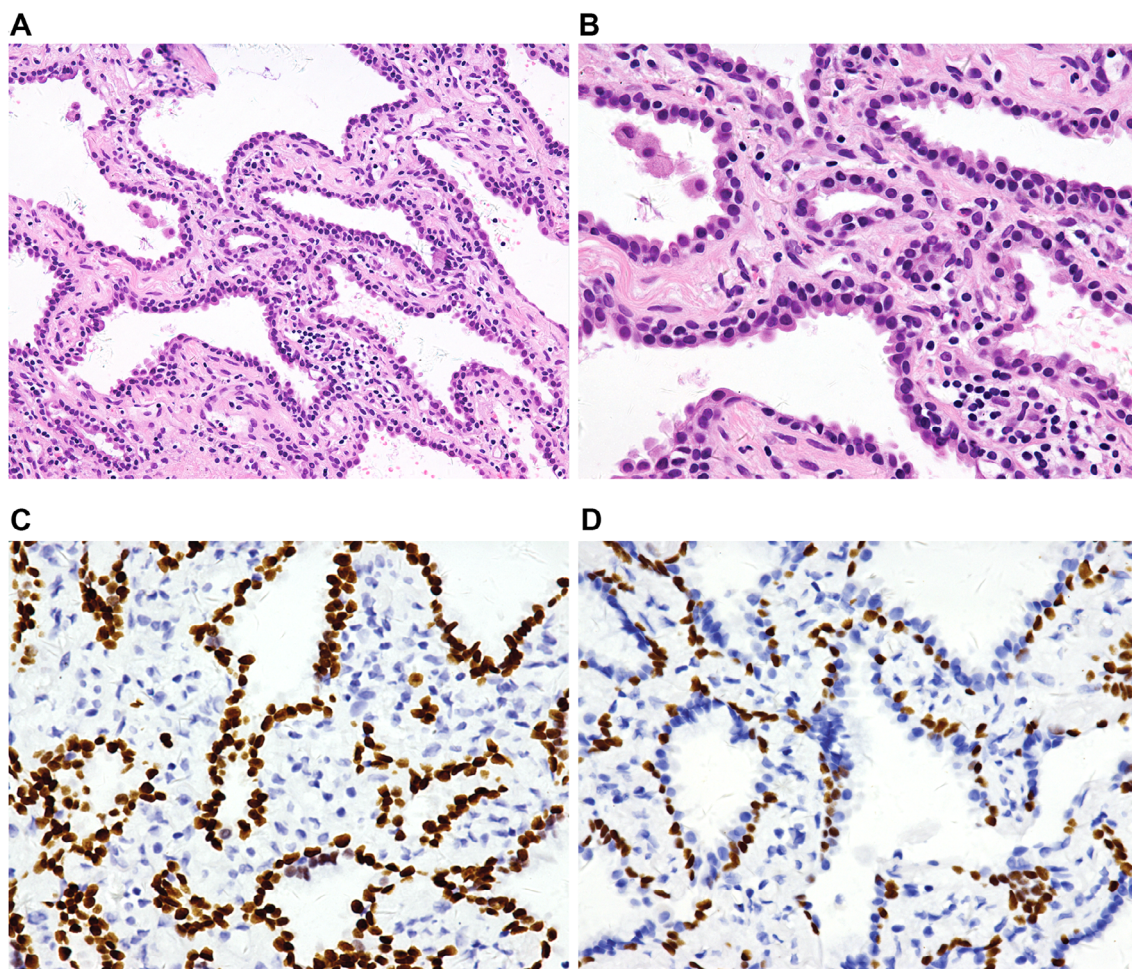
**Figure 3.** Morphological features of distal-type BAs. (A) Such tumors show a predominantly glandular structure. Papillary structures are rarely observed with minimal extracellular mucin production. (B) Luminal cells are primarily cuboidal or columnar, with Clara cells having an apical dome that is consistent with apocrine secretion. (C) TTF1 expression is detected in the luminal and basal cells. (D) p40 expression is detected in basal cells.

found at the surface of the papillary/glandular architecture, and clusters of mucinous cells were interspersed with ciliated columnar cells, with a continuous underlying layer of basal cells (Figure 1). Ciliated columnar cells expressed TTF1, whereas TTF1 expression was largely absent in mucinous cells. Only one case displayed focal areas of weakly positive TTF1 staining. Basal cells expressed TTF1, p40, p63, and CK5/6. In all cases, the expression of Ki67 was low (~1%).

The three cases of proximal-type BA fitted the description of flat, proximal-type BA. The tumors formed minimal papillary structures and displayed a predominantly flat architecture with abundant alveolar mucin. The epithelial cells were primarily composed of ciliated columnar cells and a high proportion of mucinous cells, with an underlying continuous layer of basal cells (Figure 2). Notably, in

one such case, regions that lacked a basal cell layer were observed.

Of the 18 BA cases, 7 corresponded to distal-type BAs. The luminal cells were mostly cuboidal or columnar, with an occasional appearance of ciliated columnar and mucinous cells that formed a glandular architecture and contained an underlying continuous basal cell layer (Figure 3). However, four of the distal-type BAs displayed regional monolayered structures in the absence of a basal cell layer and were composed of columnar or cuboidal cells. Some of the cells contained sparse apical cilia and a transparent cytoplasm. Moreover, the monolayered regions were continuous with the bilayered regions (Figure 4).

This study also identified eight lesions that were composed entirely of monolayered columnar or cuboidal epithelial cells, forming glandular or papillary
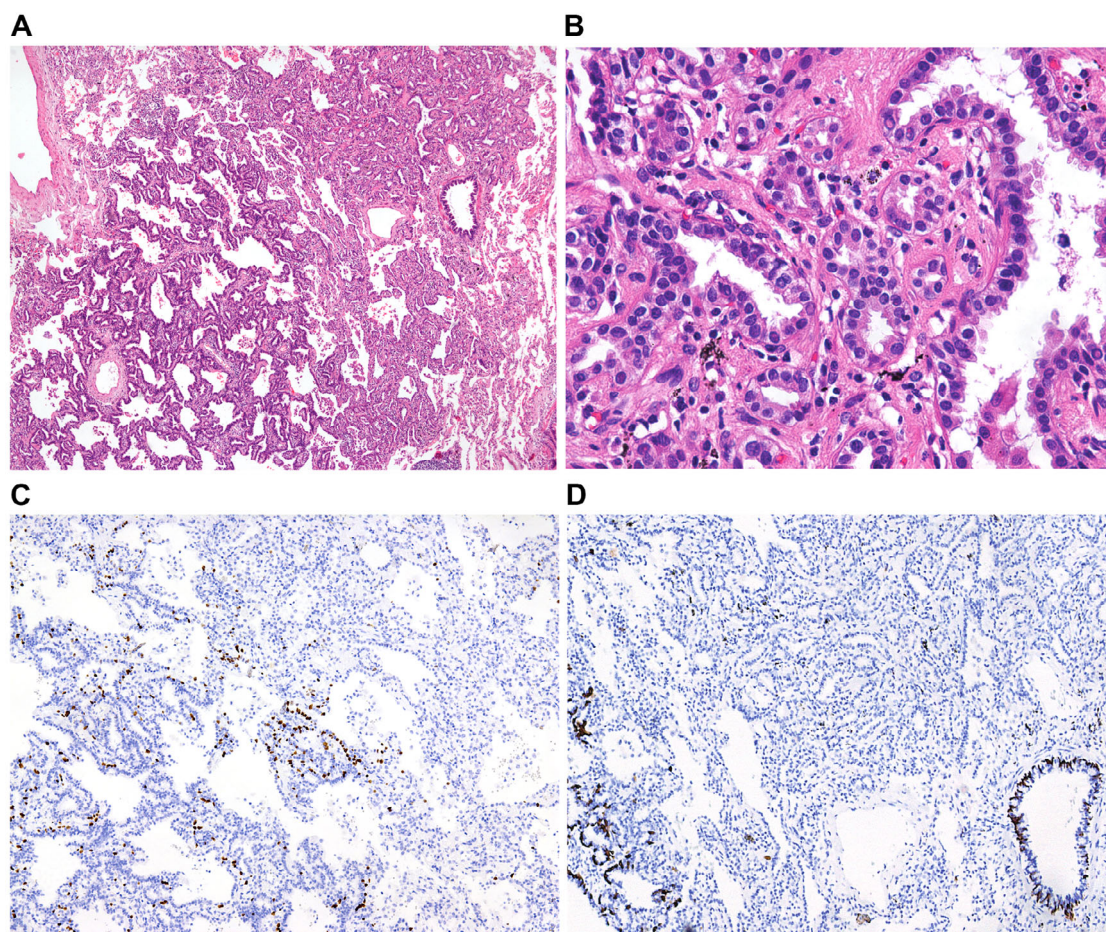
**Figure 4.** Morphological features of the mixed-type BAs with monolayered lesions. (A) The tumor tissue is composed of two distinct parts. In this case, one region of the tumor is composed of a bilayered structure with both luminal and basal cell layers, whereas the continuous region (upper right, with an enlarged view in B) is composed of only a single layer of luminal epithelial cells. (B) Some of the monolayered cells exhibit clear cytoplasm, with sparse cilia on the apical side, whereas some exhibit a mildly atypical morphology with the presence of intranuclear inclusion bodies. (C) p40 and (D) CK5/6 expression are detected only in the bilayered region of the tumor.

structures. The morphology of the epithelial cells was similar to that of the luminal cells found in classic bilayered BAs with TTF1 expression. Ciliated structures of varying abundance were frequently found on the apical surface, with a few interspersed mucinous cells. The majority of those cells exhibited minimal cytological atypia, with some having slightly enlarged nuclei. No evidence of stromal invasion was detected, and no discernible basal cell layer was observed in any of the cases. Consequently, we termed such lesions 'monolayered BA-like lesions' (Figure 5).

## Molecular profiling

Samples from 25 cases underwent NGS using a targeted panel of 422 cancer-related genes (GeneseeqPrime;

Table 1 and Figure 6A). Driver alterations were detected in 23 cases (Figure 6B and Table 2), including 13 cases (52%) with various *EGFR* mutations, 4 (16%) with *KRAS* G12D/V mutations, 3 (12%) with *BRAF* V600E mutations, 2 (8%) with *ERBB2* mutations, and 1 (4%) with a *RET* fusion. Other variants of unknown significance are also shown in Table 1 and Figure 6A, and no cancer-related mutations were detected in the two cases lacking driver mutations. *EGFR* exon 20 insertions were detected in eight patients and were the most common *EGFR* alterations. Among those eight cases, four (4/8, 50%) harbored the p.N771_H773dup mutation, and one case each harbored the p.A767_V769dup, p.S768_D770dup, p.P772_H773insYNP, and p.N771_P772insT mutations. Another case harbored compound G719S/S768I mutations. The remaining four *EGFR*-positive
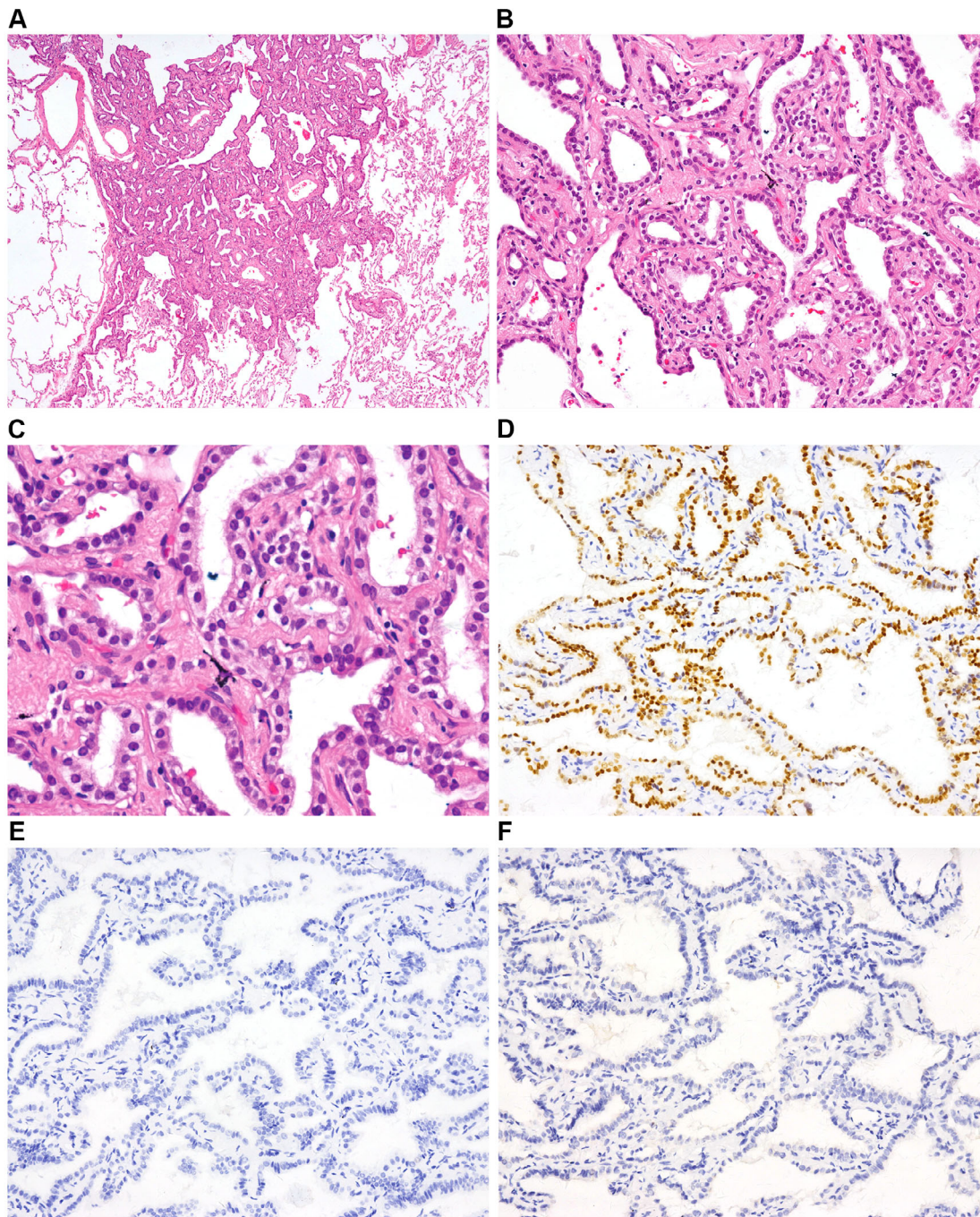
**Figure 5.** Morphological features of monolayered BA-like lesions. (A) Example of a 0.7-cm nodule in the peripheral lung. At low power, the tumor was made up of glandular or papillary structures. (B) The tumor architecture and cellular composition resemble classic BA, but it is composed entirely of monolayered columnar or cuboidal epithelial cells. (C) Ciliated structures can be seen on the apical surface of the monolayer. The tumor cells appear mildly atypical, some exhibiting a slightly increased nucleocytoplasmic ratio. (D) TTF1 is expressed on the monolayered BA-like lesion. (E) CK5/6 is completely undetected on the monolayered BA-like lesion. (F) p40 expression is also completely undetected on the monolayered BA-like lesion.
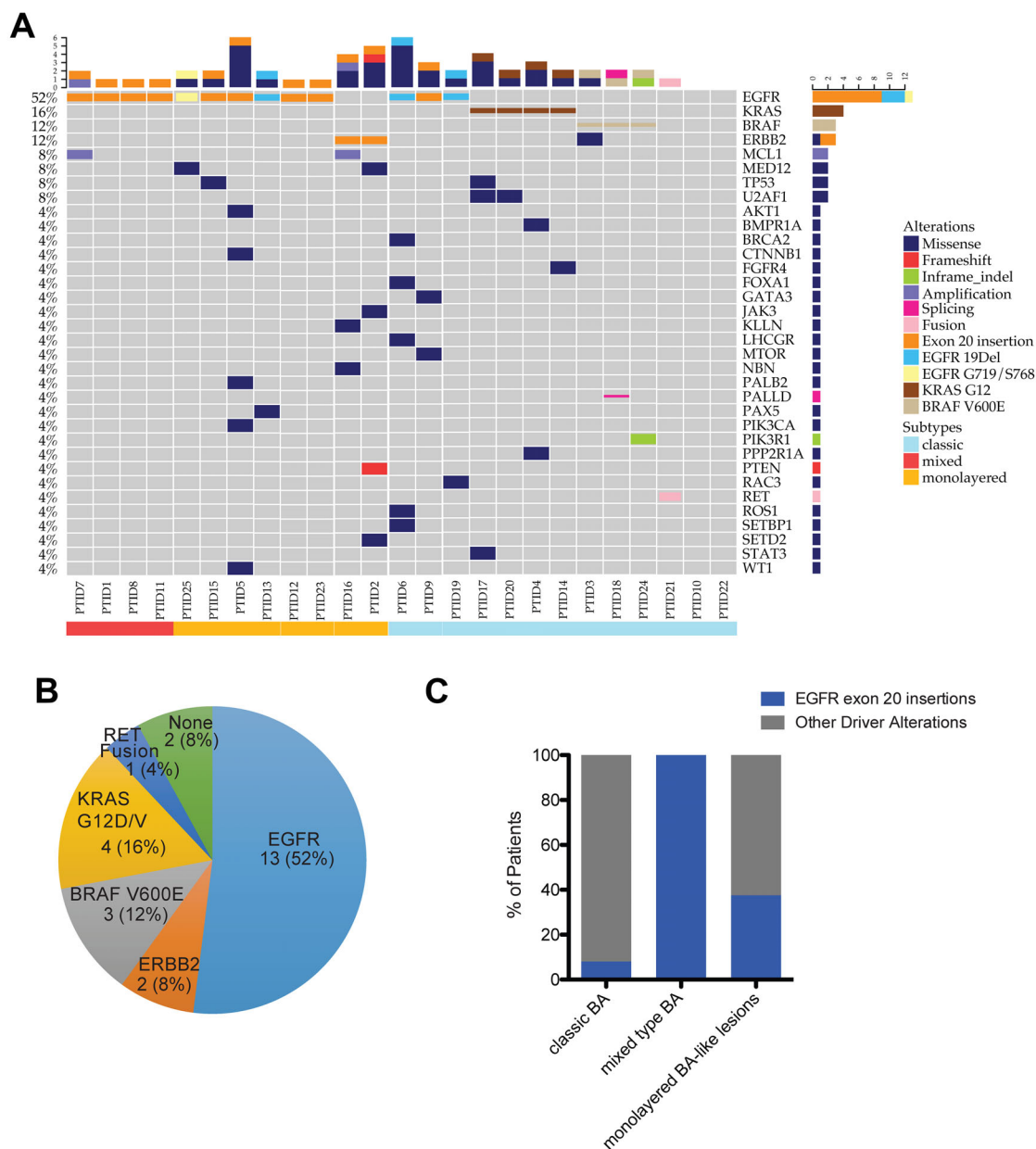
**Figure 6.** Distribution of mutations detected in the study cohort. (A) Comutation plot showing all detected mutations in each of the 25 cases that underwent targeted NGS. (B) Pie chart showing the distribution of driver mutations. (C) Comparison of the prevalence of *EGFR* exon 20 insertions in classic BA, BA with monolayered cell lesions, and monolayered BA-like lesions ($p = 0.002$, Fisher's exact test; false discovery rate = 0.014).

cases carried exon 19 deletions. The four *KRAS*-positive cases all exhibited alterations at codon 12, with two cases containing the G12V mutation and two cases containing the G12D mutation. The three *BRAF* mutations were all V600E mutations. *ERBB2* mutations included exon 20 insertions, with one case of the p. Y772_A775dup and another case with the p.

G776delinsLC mutation. The one case of *RET* fusion included *ERC1*:intron 4-*RET*:intron11. All of the driver mutations were mutually exclusive.

Notably, an *EGFR* exon 20 insertion mutation was detected in one case with classic BA (8%), four cases of BAs with monolayered cell lesions (100%), and three cases of monolayered BA-like lesions (37.5%;

Table 2. Comparisons of driver alterations between different bronchiolar lesions.

|  | Classic BA | Mixed type | Monolayered type | Total | P value (Fisher's exact test) | Adjusted P value (FDR) |
|---|---|---|---|---|---|---|
| *EGFR* 19del | 2 |  | 2 | 4 | 0.62 | 0.72 |
| *EGFR* G719/S768 |  |  | 1 | 1 | 0.48 | 0.67 |
| *EGFR* 20ins | 1 | 4 | 3 | 8 | 0.002 | 0.014 |
| *ERBB2* 20ins |  |  | 2 | 2 | 0.11 | 0.39 |
| *BRAF* V600E | 3 |  |  | 3 | 0.25 | 0.44 |
| *KRAS* G12D/V | 4 |  |  | 4 | 0.19 | 0.44 |
| *RET* fusion | 1 |  |  | 1 | 1 | 1 |
| Total with driver | 11 | 4 | 8 | 23 |  |  |
| No driver | 2 |  |  | 2 |  |  |
| Total | 13 | 4 | 8 | 25 |  |  |

FDR, false discovery rate.

$p = 0.002$, Fisher's exact test, false discovery rate = 0.014; Figure 6C). Exon 20 insertions in *ERBB2* were detected in two patients with monolayered BA-like lesions. Conversely, *EGFR* exon 19 deletions were detected in two cases of classic BAs and two cases of monolayered BA-like lesions (15 versus 25%) but were not found in patients with BAs containing monolayered cell lesions ($p = 0.62$, Fisher's exact test; Figure 6C). All other driver mutations, including *BRAF* V600E (23%), *KRAS* G12D/V (31%), and *RET* fusion (8%), were found exclusively in patients with classic BA (Figure 6B). In addition to driver mutations, we also noted a potential correlation between the presence of phosphatidylinositol 3-kinase (PI3K) pathway-activating mutations and loss of the basal layer. Overall, two of the eight cases with monolayered BA-like lesions carried PI3K pathway gene mutations that are likely pathogenic. Specifically, we detected *AKT1* (p.E17K) and *PIK3CA* (p.H1047Q) mutations in one case, both of which are cancer hotspot mutations, and a loss-of-function mutation in *PTEN* in the other case. On the other hand, the functional significance of PI3K pathway gene mutations detected in the two cases of classic BA is unclear.

## Discussion

It is currently accepted that BA with a bilayered cellular structure is a benign neoplasm that originates from the bronchiolar epithelium [2]. Based on the anatomical position in which they originated, Chang *et al* categorized BAs into proximal and distal types. Proximal-type lesions include the prototypical CMPTs, as well as those with a predominantly flat architecture. In this study, we found a high prevalence of CMPT, accounting for 44.4% (8/18) of all BA cases. The incidence of flat, proximal-type BAs was low, with only three cases. Classic CMPT is a double-layered tumor with prominent papillary architecture and abundant mucin production, which arises from proximal bronchiolar epithelium and consists of ciliated columnar cells, mucinous cells, and basal cells. The flat, proximal-type BAs are morphologically different from CMPTs in that they are mainly characterized by a glandular architecture with ciliated columnar cells and fewer mucinous cells than CMPTs, among which there are also nonciliated columnar cells. Distal-type BAs accounted for 38.9% (7/18) of all BA cases in this study, with tumors primarily composed of nonciliated cuboidal or columnar cells and only few mucinous and ciliated cells on the luminal side of the glandular architecture. Thus, our data indicate that CMPT is the most prevalent subtype of BA.

One shared feature of all types of BA is the presence of a continuous layer of basal cells underlying the glandular epithelial cells. However, we found five cases (four distal-type BAs and one proximal-type BA) that lacked a continuous basal cell layer in some regions of the lesion, which coexisted and shifted with double-layered regions. We also report eight cases that were composed of entirely monolayered columnar or cuboidal cells, which we termed monolayered BA-like lesions. These monolayered lesions formed glandular or papillary structures containing a few interspersed mucinous cells. Cilia of varying abundances were observed on the apical surface. In some regions of the lesions, absence of cilia was also observed. The epithelial cells appeared mildly atypical, with some of the cells exhibiting transparent cytoplasm and slightly increased nucleocytoplasmic ratio, as well as the presence of intranuclear inclusion bodies under high magnification. These epithelial cells were morphologically similar to the luminal cells in classic BA, despite the absence of a discernible basal cell layer. Although we

observed mild morphological atypia given the slight increase in the nucleocytoplasmic ratio in some cells, no obvious cellular atypia or lung stromal invasion was observed. Moreover, the average size of the eight monolayered BA-like lesions was 0.7 cm. Thus, their architecture and cellular morphology were entirely distinct from those of invasive adenocarcinomas. Similarly, these lesions were also morphologically distinct from adenocarcinoma *in situ* (AIS), which arises from the alveolar epithelium [6]. The neoplastic cells of AIS display features of type II pneumocytes and/or Clara cells, which grow along preexisting alveolar walls. Classic AIS generally consists of rounded or cuboidal cells with a hobnail appearance protruding into the alveolar lumen (so-called 'peg cells'). The presence of ciliated columnar cells or mucinous cells is very rare.

The presence of mild cytological atypia and lack of the basal cell layer in monolayered BA-like lesions suggest that they have the potential to transition into a malignant tumor. We propose that the three types of lesions described in this study (classic BA, BA with monolayered cell lesions, and monolayered BA-like lesions) likely reflect a continuous process of malignant transformation from benign adenoma of the bronchiolar epithelia. In our experience, we have encountered one case of invasive adenocarcinoma with partly BA and monolayered BA-like regions in the surrounding areas of the tumor (see supplementary material, Figure S1). However, whether monolayered BA-like lesions represent atypical hyperplasia of bronchiolar epithelium, a precancerous condition similar to atypical adenomatous hyperplasia of the alveolar epithelium, or whether they would eventually become AIS or even invasive adenocarcinoma warrants further large-scale investigations of similar cases.

Molecular profiling of the study cohort revealed a diverse array of oncogenic driver alterations, including *EGFR* (52%), *ERBB2* (8%), *KRAS* (16%), and *BRAF* (12%) mutations and a *RET* fusion (4%). The molecular characteristics of our classic BA cohort were consistent with the BA cohort reported by Chang *et al* [2], with the incidence of *BRAF* V600E, *KRAS* G12D/V, and *EGFR* mutations being 23, 31, and 23%, respectively, in this study. The association between *RET* fusion and BA was previously unreported.

The overall incidence of *EGFR* mutations in our BA cohort was 52%, which was comparable to the ~50% prevalence of *EGFR* mutations in non-small-cell lung cancer (NSCLC) patients of the East Asian population [7,8]. In contrast to an overall incidence of *EGFR* mutations of 4–10% in NSCLC cases [9], *EGFR* exon 20 insertions in BA samples and its variants accounted for 61.5 and 50% of the total *EGFR*-positive cases in this

study and that of Chang *et al*'s study [2], respectively. In this study, p.N771_H773dup was the most prevalent (4/13; 30.8%) form of *EGFR* mutation and represented 50% of *EGFR* exon 20 insertions. By contrast, the incidence of p.N771_H773dup was ~0.5% in lung adenocarcinoma, which is equivalent to 8% of all *EGFR* exon 20 insertions [2,10]. In addition to BA and its variants, there are other benign tumors that are enriched with *EGFR* exon 20 insertions, particularly p.N771_H773dup, including fibrous hamartoma of infancy [11] and inverted sinonasal papilloma [12]. p.A767_V769dup and p.S768_D770dup occurred once each in our cohort and were undetected in the Chang *et al*'s cohort. By contrast, p.A767_V769dup and p.S768_D770dup insertions are the most common subtypes of *EGFR* exon 20 insertions in NSCLC, with an incidence of 21 and 20%, respectively, which correspond to a prevalence of 0.4–0.8% in NSCLC [9]. The incidence of p.P772_H773insYNP and p.N771_P772insT in lung adenocarcinomas is low (<0.1%) and has only been reported in a few cases [13-15].

Notably, we also observed significant genetic differences among BA and its variants (BA with monolayered cell lesions and monolayered BA-like lesions), with a marked enrichment of *EGFR* exon 20 insertions in the BA variants. *EGFR* exon 19 deletions were found in two cases of BAs and two cases of monolayered BA-like lesions (15 versus 25%, respectively). The specific subtypes of *EGFR* exon 19 deletions included p.E746_S752delinsA, p.L747_A755>GD, p.E746_L747>IP, and p.E746_A750del, which are non-overlapping with the mutations described in the Chang *et al*'s report (p.E746_S752>V and p.L747_S752del) [2]. The two cases of *ERBB2* mutations were exon 20 insertions, including p.Y772_A775dup and p.G776delinsLC, which both occurred in patients with monolayered BA-like lesions. *ERBB2* exon 20 insertions occurred in 2–4% of lung cancers, and the reported frequencies of p.Y772_A775dup and p.G776delinsLC are approximately 60% and 5% of all *ERBB2* exon 20 insertions in NSCLC, respectively [16-18]. High-throughput sequencing also revealed a number of co-occurring mutations and likely pathogenic PI3K pathway gene mutations in two cases of monolayered BA-like lesions. However, given the limited follow-up time and sample size, the clinical and biological significance of specific driver and co-occurring alterations remains to be explored.

In conclusion, the morphological, immunohistochemical, and genetic characteristics of the 13 classic BA cases in this study were consistent with those reported in previous studies [2]. In the five BA cases

with a regional discontinuous basal cell layer and the eight cases that were morphologically indistinguishable from distal-type BAs – with the exception of the absence of a basal cell layer – we found a high proportion of *EGFR* exon 20 insertions. Furthermore, the overall genetic characteristics of these BA variants were considerably different from those of classic BAs and lung adenocarcinomas.

## Author contributions statement

JS, HB, JCY and XW analyzed and interpreted the clinical and sequencing data. RZ and LZ collected patient samples and clinical information. YH performed histological examination of the lesions. JZ, YS and XW supervised the study. JS, JCY and JZ wrote the manuscript with the help of all authors.

## References

1. Kamata T, Yoshida A, Kosuge T, *et al*. Ciliated muconodular papillary tumors of the lung: a clinicopathologic analysis of 10 cases. *Am J Surg Pathol* 2015; **39:** 753–760.
2. Chang JC, Montecalvo J, Borsu L, *et al*. Bronchiolar adenoma: expansion of the concept of ciliated muconodular papillary tumors with proposal for revised terminology based on morphologic, immunophenotypic, and genomic analysis of 25 cases. *Am J Surg Pathol* 2018; **42:** 1010–1026.
3. McKenna A, Hanna M, Banks E, *et al*. The Genome Analysis Toolkit: a MapReduce framework for analyzing next-generation DNA sequencing data. *Genome Res* 2010; **20:** 1297–1303.
4. Koboldt DC, Zhang Q, Larson DE, *et al*. VarScan 2: somatic mutation and copy number alteration discovery in cancer by exome sequencing. *Genome Res* 2012; **22:** 568–576.
5. Amarasinghe KC, Li J, Hunter SM, *et al*. Inferring copy number and genotype in tumour exome data. *BMC Genomics* 2014; **15:** 732.
6. Travis WD, Brambilla E, Noguchi M, *et al*. International Association for the Study of Lung Cancer/American Thoracic Society/European Respiratory Society international multidisciplinary classification of lung adenocarcinoma. *J Thorac Oncol* 2011; **6:** 244–285.
7. Shi Y, Au JS, Thongprasert S, *et al*. A prospective, molecular epidemiology study of EGFR mutations in Asian patients with advanced non-small-cell lung cancer of adenocarcinoma histology (PIONEER). *J Thorac Oncol* 2014; **9:** 154–162.
8. Midha A, Dearden S, McCormack R. EGFR mutation incidence in non-small-cell lung cancer of adenocarcinoma histology: a systematic review and global map by ethnicity (mutMapII). *Am J Cancer Res* 2015; **5:** 2892–2911.
9. Vyse S, Huang PH. Targeting EGFR exon 20 insertion mutations in non-small cell lung cancer. *Signal Transduct Target Ther* 2019; **4:** 5.
10. Zehir A, Benayed R, Shah RH, *et al*. Mutational landscape of metastatic cancer revealed from prospective clinical sequencing of 10,000 patients. *Nat Med* 2017; **23:** 703–713.
11. Park JY, Cohen C, Lopez D, *et al*. EGFR exon 20 insertion/duplication mutations characterize fibrous hamartoma of infancy. *Am J Surg Pathol* 2016; **40:** 1713–1718.
12. Udager AM, Rolland DCM, McHugh JB, *et al*. High-frequency targetable EGFR mutations in sinonasal squamous cell carcinomas arising from inverted sinonasal papilloma. *Cancer Res* 2015; **75:** 2600–2606.
13. Arcila ME, Nafa K, Chaft JE, *et al*. EGFR exon 20 insertion mutations in lung adenocarcinomas: prevalence, molecular heterogeneity, and clinicopathologic characteristics. *Mol Cancer Ther* 2013; **12:** 220–229.
14. Wu JY, Wu SG, Yang CH, *et al*. Lung cancer with epidermal growth factor receptor exon 20 mutations is associated with poor gefitinib treatment response. *Clin Cancer Res* 2008; **14:** 4877–4882.
15. Riess JW, Gandara DR, Frampton GM, *et al*. Diverse EGFR exon 20 insertions and co-occurring molecular alterations identified by comprehensive genomic profiling of NSCLC. *J Thorac Oncol* 2018; **13:** 1560–1568.
16. Arcila ME, Chaft JE, Nafa K, *et al*. Prevalence, clinicopathologic associations, and molecular spectrum of ERBB2 (HER2) tyrosine kinase mutations in lung adenocarcinomas. *Clin Cancer Res* 2012; **18:** 4910–4918.
17. Kris MG, Camidge DR, Giaccone G, *et al*. Targeting HER2 aberrations as actionable drivers in lung cancers: phase II trial of the pan-HER tyrosine kinase inhibitor dacomitinib in patients with HER2-mutant or amplified tumors. *Ann Oncol* 2015; **26:** 1421–1427.
18. Liu Z, Wu L, Cao J, *et al*. Clinical characterization of ERBB2 exon 20 insertions and heterogeneity of outcomes responding to afatinib in Chinese lung cancer patients. *Onco Targets Ther* 2018; **11:** 7323–7331.

---

## SUPPLEMENTARY MATERIAL ONLINE

**Figure S1.** Invasive adenocarcinoma with partly BA and monolayered BA-like regions

**Table S1.** The 422 cancer-related genes included in the GeneseqPrime Panel

---